Supplemental Material

Simulated diagenesis of the iron-silica precipitates in banded iron formations

Isaac L. Hinz, Leanne Rossi, Chi Ma, and Jena E. Johnson

Preparation of Experimental Solutions

The solution pH was carefully controlled during the experimental set-up. The pH was momentarily adjusted to 3 to add salts expected for the Archean ocean (Table 1) until they were fully dissolved. Ferrous chloride tetrahydrate was also added using a 300 mM stock at pH 3 to avoid pH-driven precipitation of Fe(II) phases. The pH was then readjusted to ~5 with 1 M sodium hydroxide (NaOH) to limit the exsolution of CO_2 (aq) at pH < 5 before the addition of our sodium bicarbonate buffer. The bicarbonate buffer was added to the solution dropwise, gradually increasing the solution pH until around pH 6.7-6.9 where it was held by 1 M HCl and 1 M NaOH additions to keep the pH ≤ 7. After the bicarbonate buffer was added, the solution was readjusted back to pH 7 at 15 minute intervals for 2 hours, as the solution had the tendency to drift to pH 7.2-7.3 over time. The stir bar was removed from the bottle to limit nucleation. The duplicate 3.6 L solutions were gently mixed together three times in 4 L jugs to create one homogeneous bulk solution (total 7.2 L) that was measured to have a pH of 7.0 prior to experimentation. Final silica concentrations were measured using the silicomolybdate assay (Strickland and Parsons 1972).

The bulk solution was then transferred as 510 mL portions to 610 mL borosilicate glass bottles. Each bottle was outfitted with a 1.5 mm chemically resistant silicone rubber seal nested in a Restek™ GL-45 Mobi-Cap with two ¼″-28 threaded ports (Restek™ #27835). The bottles were then split into an experimental, bubbled set and a control set. Both were ultimately stored laying on their side to prevent any contact with O_2 contamination in the glovebox air and optimize contact with the headspace.

Bubbling with ppm-level O_2

The six sealed experimental bottles were transported to a multi-valve gassing station. Two ¼″ -28 threaded screws were removed to expose a small portion of the silicone rubber seal. We next connected a 4″ needle to the multi-valve gassing station to provide N_2 mixed with 49.1 ± 0.9 ppm O_2, puncturing through the silicone rubber seal in port 1 to bubble gas into the solution. Then, a separate 2″ needle was quickly punctured through port 2 of the silicone rubber seal to allow for gas exchange and pressure relief of the system. The bottles were continuously bubbled for 90 minutes at 3 psi to ensure full exchange of the headspace.

Solution samples from each experiment were extracted at 15 minute intervals and the pH was measured on a ThermoFisher Orion Star A221 pH meter outfitted with a Fisherbrand accuCap spear tipped capillary junction pH probe. With every 15 minutes of bubbling, the pH of the system increased by an average of 0.09 units, likely due to the exsolution of CO_2(aq)/$H_2CO_3^*$. To mitigate this effect, anoxic 2 M HCl was added in dropwise to readjust the pH back to 7 during O_2 bubbling.

Supplemental Material

After 90 minutes, the 2″ pressure relief needle was removed, quickly sealed with the screw followed by the 4″ gassing needle being removed and sealed with a screw to lock in the headspace. The upright bottle was then tilted 90° to maximize the headspace-solution contact and limit any unwanted interaction of O_2 from the surrounding environment. The tilted bottles were transported back into the glovebox and remained resting on their side wrapped in aluminum foil.

Because the bubbled experiments were equilibrated at 49 ppm O_2 by continued bubbling of this oxygen over 1.5 hours, their oxygen fugacity ($f(O_2)$) was set to $10^{-4.3}$ atm (equivalent to an oxygen fugacity, log $f(O_2)$, of 0.7 Pa). In contrast, the control experiments were purged with pure N_2 and were therefore more reducing. The iron metal in the stainless-steel Parr vessels may have further buffered the experiments to even more reducing conditions over the course of the hydrothermal aging experiments.

In addition to barometric pressure (0.96 atm in Ann Arbor, MI), we estimate that the maximum vapor pressure experienced during simulated diagenesis was 0.5 atm at 80 °C, 4.7 atm at 150 °C, and 23 atm at 220 °C, with the ions in solution likely lowering the overall saturation vapor pressure. Therefore, the total pressure at each temperature of 80 °C, 150 °C, and 220 °C, was approximately 1.5 atm, 5.7 atm, and 24 atm, respectively.

Ferrous Iron Analysis: Wilson Vanadate Method

We modified the Wilson method from Andrade et al. (2002) to analytically determine percent ferrous iron in a sample (also see Ammonette and Scott 1991; Wilson 1955). The method was adapted to fit the capabilities of the lab, including substituting hydrofluoric acid with sulfuric acid and acid digestion at room temperature instead of in a hot water bath. To first validate our modifications of this method, we followed the Andrade et al. protocol on three rounds of ferrous ammonium sulfate standards stored in a desiccator (Table S2). One additional set of these standards, performed after the samples, tested the accuracy of the method on the low FeII masses that we obtained from the samples. All the standard powders were weighed using an Ohaus Explorer scale prior to dissolution.

Subsamples of the bubbled samples, which had sufficient remaining solid material for the Wilson vanadate assay, were extracted in the glovebox. We note that this material had been stored in the glovebox at room temperature for >6 months so secondary reactions may have occurred. First, anoxic 18.2 MΩ-cm ultrapure water was added to each sample to form a slurry. We then transferred the slurries to a pre-weighed 1.5 mL Eppendorf tube and allowed the samples to dry in the glovebox at room temperature with the Eppendorf tube cap off. Subsequently, we weighed the samples in a closed Eppendorf tube on the benchtop before returning to the glovebox for anoxic dissolution.

Samples and standards were transferred to a 100mL glass bottle with a screw top cap and mixed with 5mL of 1% ammonium metavanadate in 0.9 M sulfuric acid, 40mL of 85% o-phosphoric acid, and 5mL of ~98.0% sulfuric acid. The solution was gently mixed in between each addition. Each sample or standard was then left to dissolve for 2 hours. We additionally prepared a blank with each round of the titration. For the oxygen-sensitive samples, this dissolution was performed in the glovebox. Additionally, a pre-weighed 0.1 g internal standard of ferrous ammonium sulfate was included in the sample series.

Supplemental Material

To all the standards, blanks, and the pre-dissolved sample set, we added 10 mL of a 1:2:2 solution of phosphoric acid, sulfuric acid, and 18.2 MΩ-cm ultrapure water. Next, we mixed with 100 mL saturated boric acid in an empty 500 mL Erlenmeyer flask. The bottles were rinsed twice with 50 mL saturated boric acid to ensure all sample residue was removed from the bottle. Finally, 10 mL of 2% ferrous ammonium sulfate and 1 mL of 0.2% (w/v) barium diphenylamine sulfonate were added one at a time to all bottles and mixed. We then titrated with 0.1 N potassium dichromate until the solutions reached a deep purple endpoint, upon which we recorded the final volume.

The dichromate titrant volume was used to convert to % FeII. Following Andrade et al., we subtracted the titrant volume of the blank from the sample, multiplied the sum by the normality of the potassium dichromate, and then multiplied that by the product of 5.5847 (a factor to transform dichromate volume into % FeII by mass). The product was then divided by the mass of the sample to get %FeII or divided by 100 to obtain the measured mass of FeII, which was useful for comparing the ferrous ammonium sulfate standards to their theoretically calculated FeII by total mass (Table S2, Table S3).

Thermodynamic modeling of mineral stability fields

Within the Act2 module in Geochemist's Workbench, we added the relevant ion constituents of our basal solution (Table 1). We assumed that activity was approximately the same as the initial concentration, but we note the salinity and precipitation reactions would have altered these numbers—perhaps substantially in the case of Fe and Si as they were major components of the precipitates. Nevertheless, these thermodynamic stability plots should be informative to obtain a sense of the stable phases in the general chemical framework of our experimental system. Additionally, we modified the temperature and pressure according to our experimental set-up and pressure estimates given above (1.5 atm at 80 °C, 5.7 atm at 150 °C, 24 atm at 220 °C). We plotted magnesium and iron aqueous complexes and minerals to obtain insights into the precipitates in the control and bubbled experiments. To make the diagrams clear and focus on solid phases that were plausible and characterizable, we suppressed a number of dissolved species: Fe- and Mg-acetate complexes(5), Fe-Cl complexes (6) and Fe-OH species (2). We also suppressed highly crystalline minerals that are commonly more stable than their precursor minerals and would be more likely for us to observe in our experiments. These suppressed solids were: Ferrite-Mg, Hematite, Lawrencite, Minnesotaite, Molysite, $NaFeO_2$, FeO, and Talc (which was shown on Fig. S1a).

The Mg stability field diagrams indicated that Mg is most stable as a dissolved species at 25 °C and 80 °C at circumneutral pH (Fig. S1a-b), consistent with our observations of little precipitated Mg in the bubbled experiments and no precipitates in the control experiments at these temperatures. However, at 150 °C, the magnesite field expands (Fig. S1c), suggesting that magnesite should have been observed at this temperature. The lack of magnesite in our experiments points to kinetic controls precluding magnesite precipitation and/or the preferred association of magnesium with silica. The magnesium serpentine phase that we observe at 150 °C would be consistent with antigorite or chrysotile, which appear to be stable at slightly higher pH values than our bulk solution (Fig. S1c). Notably, our observations of chrysotile after 220 °C aging is consistent with its thermodynamic stability field (albeit only if talc and antigorite are

Supplemental Material

suppressed), suggesting that the solution and mineral assemblage may be at equilibrium (Fig. S1d).

The Fe stability field diagram did not match our experimental observations well, indicating the importance of kinetic controls on solid precipitation and microenvironment with different chemistry and redox states. We also note that we used the embedded thermodynamic dataset for Geochemist's Workbench, which does not reflect solubility data on a potential precursor greenalite phase by Tosca et al. (2016). The initial assemblage would be predicted to be a ferric oxide if there was sufficient oxidation or siderite if conditions were adequately reducing (Fig. S2a), yet we observed a mixed assemblage of abundant Fe(II)-containing silicates (based on the Fe(III)/FeT and Fe(II)/g data) and ferrihydrite. After 80 °C aging, the pH dropped slightly and the stability diagram again predicts either siderite or goethite, a representative Fe(III) oxide, with only a narrow range of Eh (redox) conditions stabilizing the observed magnetite (Fig. S2b). Upon 150 °C aging, the prevalence of magnetite is more expected for the solution pH but our observed assemblage of Fe(II)-rich greenalite, Fe(II,III) magnetite, and Fe(III) ferrihydrite is clearly not at equilibrium as it encompasses a wide range of redox potentials (Fig. S2c). Similarly, the greenalite stability field is shifted to higher pH than our measured value. A similar dichotomy is observed for the 220 °C stability diagram when compared with our observations: the greenalite, magnetite, and ferrihydrite mixture that we observed is not possible according to thermodynamics (Fig. S2d). Furthermore, greenalite should not be stable at such a low pH of <6.

References

Amonette, J.E., and Scott, A.D. (1991) Determination of ferrous iron in non-refractory silicate minerals: 1. An improved semi-micro oxidimetric method. Chemical Geology, 92, 329–338.

Andrade, S., Hypolito, R., Ulbrich, H.H.G.J., and Silva, M.L. (2002) Iron(II) oxide determination in rocks and minerals. Chemical Geology, 182, 85–89.

Strickland, J.D.H., and Parsons, T.R. (1972) A Practical Handbook of Seawater Analysis, 2nd edition. doi: 10.25607/OBP-1791.

Wilson, A.D. (1955) A new method for the determination of ferrous iron in rocks and minerals. Bulletin of the Geological Survey of Great Britain, 9, 56–58.

Supplemental Material

Tables and Figures

	Mass	Fe part	Start	End	Total Titrant	FeII conversion ((Titrant-Blank) * Normality K2Cr2O7 * 5.5847)	FeII mass (measured)	compared to actual FeII	% FeII (divided by mass)
Set 1 blank	0	0	1.29	2.5	1.21				
Ferrous ammonium sulfate	0.1019	0.01451179	2.5	6.29	3.79	1.4408526	0.01440853	0.99288407	14.1398685
Ferrous ammonium sulfate	0.2015	0.02869603	6.29	12.61	6.32	2.8537817	0.02853782	0.99448645	14.1626883
Ferrous ammonium sulfate	0.3027	0.04310814	12.61	21.23	8.62	4.1382627	0.04138263	0.95997253	13.6711685
Set 2 blank	0	0	0	0.98	0.98				
Ferrous ammonium sulfate	0.1057	0.01505296	6.99	10.51	3.52	1.4185138	0.01418514	0.94234895	13.4201873
Ferrous ammonium sulfate	0.2029	0.02889541	10.51	16.47	5.96	2.7811806	0.02781181	0.96249907	13.7071493
Ferrous ammonium sulfate	0.3026	0.0430939	16.47	24.46	7.99	3.9148747	0.03914875	0.90845227	12.9374577
Set 3 blank	0		0	1.05	1.05				
Ferrous ammonium sulfate	0.1013	0.01442634	1.05	4.69	3.64	1.4464373	0.01446437	1.00263611	14.2787493
Ferrous ammonium sulfate	0.1077	0.01533778	4.69	8.5	3.81	1.5413772	0.01541377	1.0049545	14.311766
Set 4 blank			0	0.97					
Ferrous ammonium sulfate	0.0101	0.00143836	0	1.22	0.25	0.1396175	0.00139618	0.97067011	13.8235149
Ferrous ammonium sulfate	0.0107	0.00152381	0	1.22	0.25	0.1396175	0.00139618	0.91624001	13.0483645

Table S1: Wilson vanadate method on weighed standards of ferrous ammonium chloride to confirm accuracy of this protocol. The volume of titrant is converted to weight of Fe(II) following Andrade et al. (2002) and comparisons of the measured versus actual Fe(II) mass (in g) are shown in green and blue columns, respectively. We also include the % Fe(II)/g (yellow column) to compare the determined % Fe(II) to the theoretical % of Fe(II) in ferrous ammonium sulfate, which is 14.24%. Note that set 4 was performed after the samples in order to test the accuracy of approximate amount of Fe(II) as the samples contained.

	Mass	Fe part	Start	End	Total Titrant	FeII conversion ((Titrant-Blank) * Normality K2Cr2O7 * 5.5847)	FeII mass (measured)	compared to actual FeII	% FeII (divide by mass)
Sample blank	0	0	0	0.88	0.88				
Bubb_21day 25C	0.0029		0	1.13	1.13	0.1396175	0.001396175		48.14396552
Bubb_7day 80C	0.0017		0	1.05	1.05	0.0949399	0.000949399		55.847
Bubb_7day 150C	0.0026		0	1.03	1.03	0.0837705	0.000837705		32.21942308
Bubb_7day 220C	0.0024		0	1	1	0.0670164	0.000670164		27.9235
Ferrous ammonium sulfate std	0.1038	0.014782374	0.88	4.5	3.62	1.5302078	0.015302078	1.035157016	14.74188632

Table S2: Results from applying the Wilson vanadate method on bubbled samples to obtain an estimate of their % Fe(II) by mass. Compare ferrous ammonium sulfate standard to theoretical % Fe(II)/g of 14.24%, and compare samples to theoretical % Fe(II)/g for magnetite (24%), cronstedtite (28%), and greenalite (45%).

[as separate file]
Table S3: Compiled TEM EDS data from the six analyzed experimental conditions, including raw data and corrected phase averages from various maps.

Supplemental Material

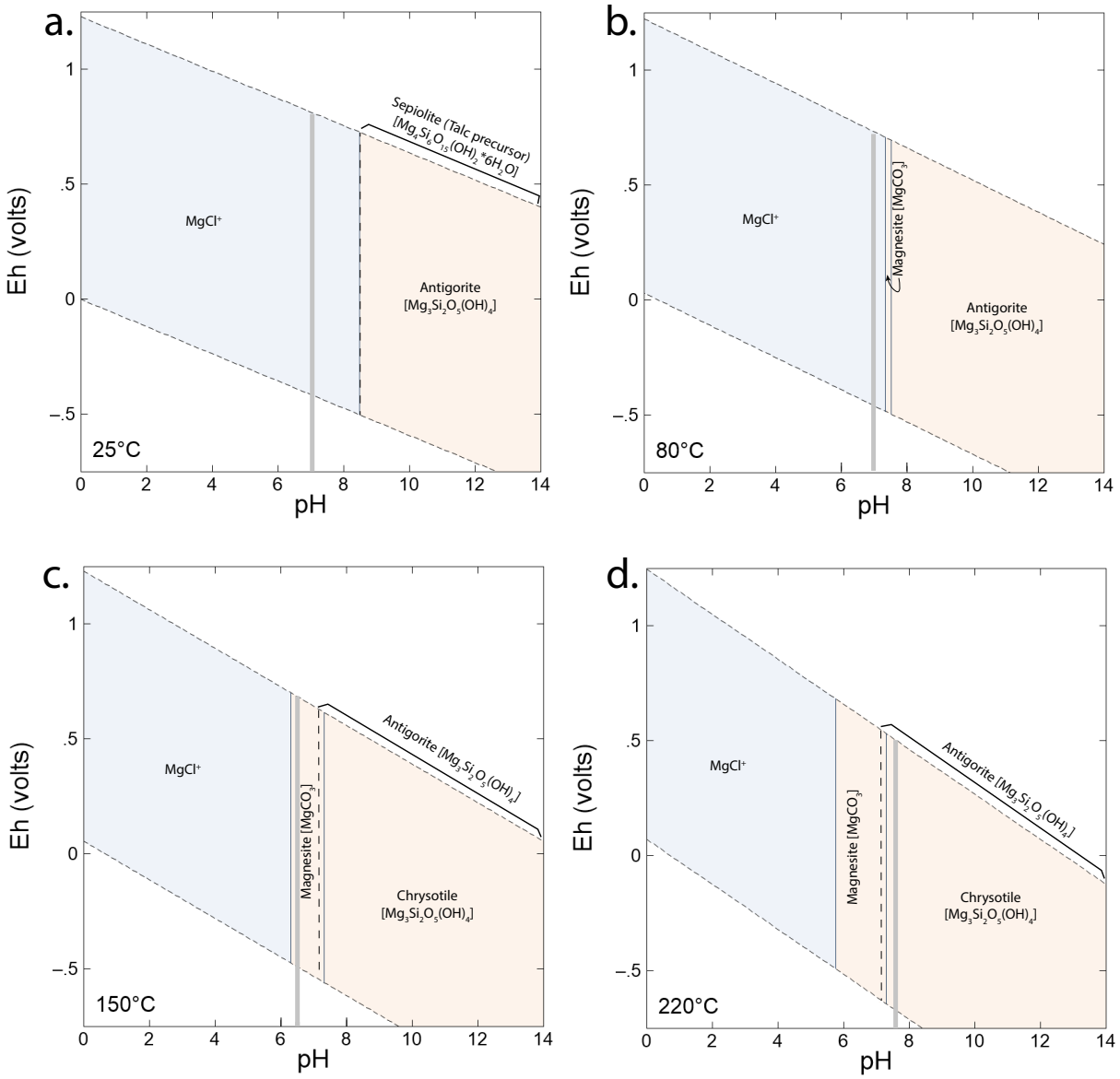

Figure S1: Magnesium stability diagrams across experimental diagenesis: (a) at 25 °C and 1 atm; (b) at 80 °C and 1.5 atm; (c) at 150 °C and 5.7 atm; (d) at 220 °C and 24 atm. Plots constructed in Geochemist's Workbench indicating the stability fields of magnesium phases across pH (0-14) and redox potential Eh (within the stability limits of water). See SM text for details on input parameters and suppressed phases. Talc and antigorite fields indicated by dashed line and upper bracket in Fig. S1a and Fig. S1c-d, respectively.

Supplemental Material

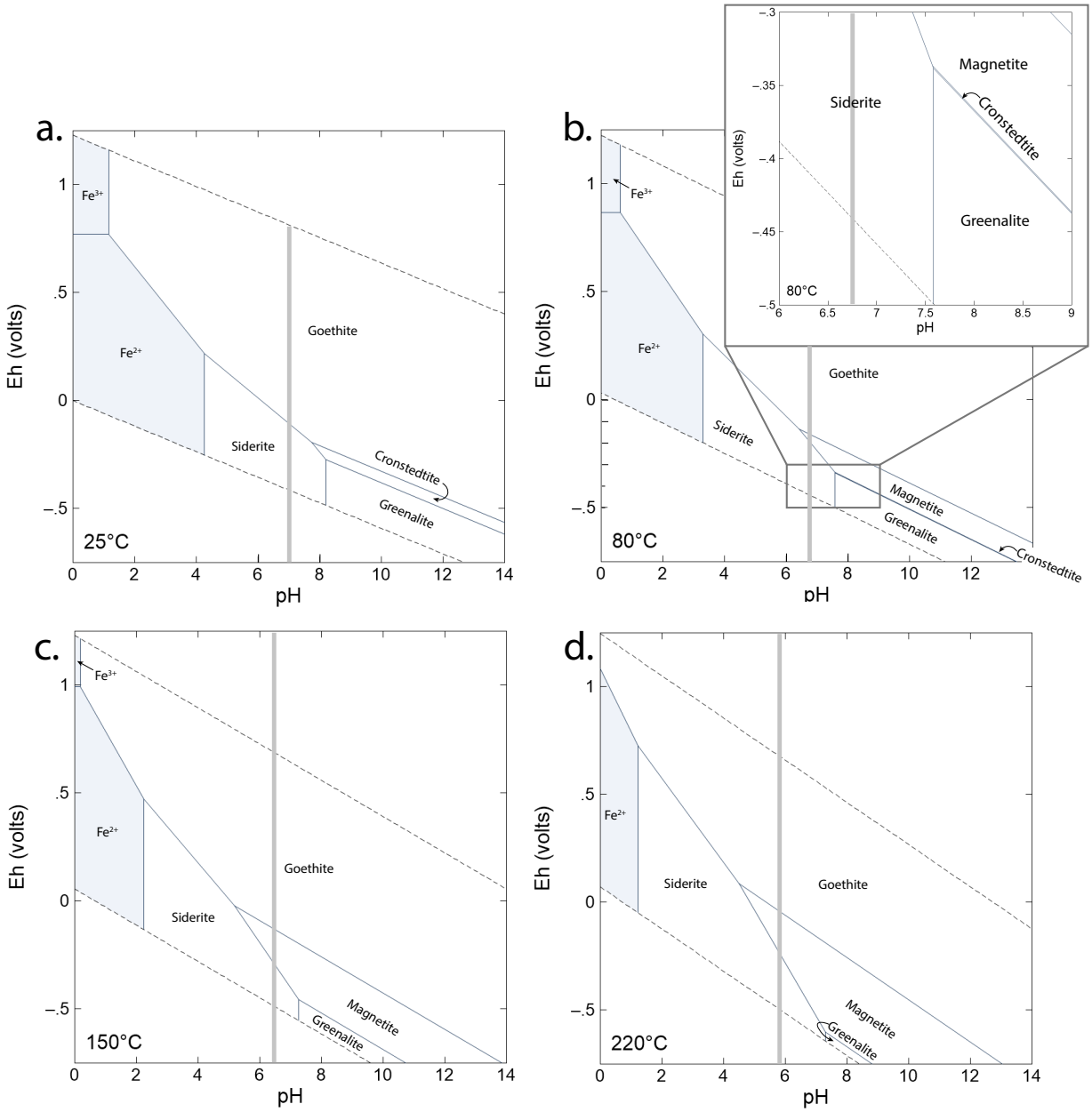

Figure S2: Iron stability diagrams across experimental diagenesis: (a) at 25 °C and 1 atm; (b) at 80 °C and 1.5 atm; (c) at 150 °C and 5.7 atm; (d) at 220 °C and 24 atm. Plots constructed in Geochemist's Workbench indicating the stability fields of iron phases across pH (0-14) and redox potential Eh (within the stability limits of water). (b) has zoom-in to indicate narrow cronstedtite field. See SM text for details on input parameters and suppressed phases.